

Molecular BioSystems

Accepted Manuscript



This is an *Accepted Manuscript*, which has been through the Royal Society of Chemistry peer review process and has been accepted for publication.

Accepted Manuscripts are published online shortly after acceptance, before technical editing, formatting and proof reading. Using this free service, authors can make their results available to the community, in citable form, before we publish the edited article. We will replace this *Accepted Manuscript* with the edited and formatted *Advance Article* as soon as it is available.

You can find more information about *Accepted Manuscripts* in the [Information for Authors](#).

Please note that technical editing may introduce minor changes to the text and/or graphics, which may alter content. The journal's standard [Terms & Conditions](#) and the [Ethical guidelines](#) still apply. In no event shall the Royal Society of Chemistry be held responsible for any errors or omissions in this *Accepted Manuscript* or any consequences arising from the use of any information it contains.



www.rsc.org/molecularbiosystems

**Identification of potential dual agonists of FXR and TGR5 using e-pharmacophore based
virtual screening**

Thangaraj Sindhu and Pappu Srinivasan*

Molecular Biology Lab, Department of Bioinformatics, Alagappa University, Karaikudi,
Tamilnadu- 630004, India

***Corresponding author**

Dr. P. Srinivasan, M.Sc., Ph.D.

Assistant Professor

Tel: +91-4565-230725

Mobile: +91-9444482814

E-mail: sri.bioinformatics@gmail.com

Abstract

Farnesoid X receptor and Takeda G-protein-coupled receptor-5 are well known bile acid receptors, act as promising target for the drug development and treatment of diabetes. Both the bile acid receptor agonists increase insulin sensitivity and control glucose, lipids and bile acid homeostasis. The current study deals with the identification of novel dual agonist using ligand and structure based virtual screening. Initially, experimentally proved well-known dual agonist of FXR and TGR5, namely, INT-767 was docked into the binding site of FXR and TGR5 to depict the protein residues important for ligand binding. The docked complexes FXR_{INT-767} and TGR5_{INT-767} were used to generate e-pharmacophore hypotheses. Ligand based virtual screening was carried out using the hypothetical e-pharmacophore model against ChemBridge database. Further, structure based virtual screening was performed with screened hits to find potential agonists of FXR and TGR5. A total of four best agonists were identified based on their affinity and mode of interactions with the receptors. Binding mode of these compounds with both the receptors was analyzed in detail. Furthermore, molecular dynamics, ADME toxicity prediction, density functional theory and binding free energy calculations were carried out to rank the compounds. Based on the above analyses, the best potent compound ChemBridge_9149693 was selected for further *in vitro* studies. The results of *in vitro* assays suggested that ChemBridge_9149693 is a most potent and promising drug for the treatment of type II diabetes. Thus, the compound could be used for further drug design and development of dual agonists of FXR and TGR5.

Keywords: FXR, TGR5, e-pharmacophore mapping, binding free energy, molecular dynamics simulation

Introduction

Farnesoid X receptor (FXR), a member of nuclear hormone receptor super family of ligand activated transcription factors and highly expressed in kidney, liver, intestine and the adrenal glands^{1,2}. FXR can be activated by the hydrophobic bile acids, including chenodeoxycholic acid (CDCA), cholic acid (CA) and deoxycholic acid (DCA)³. It has an important role in controlling glucose, lipids and bile acid homeostasis by regulating the expression of enzymes involved in the bile acid synthesis⁴. Activation of FXR by bile acids (BA) or semi-synthetic agonists lowers plasma triglycerides by the modulation of glucose induced lipogenic genes and repression of hepatic SREBP-1c expression. Previous reports indicate that BA regulates energy expenditure in a FXR-independent manner in mice through the activation of TGR5^{5,6}. Activation of FXR helps to treat liver fibrosis, diabetes, atherosclerosis, cholesterol gallstone disease, erectile dysfunction, obesity, metabolic syndrome and inflammatory bowel disease^{7,8}.

Takeda G-protein-coupled receptor-5 (TGR5), a G-protein coupled receptor plays a key role in energy and glucose homeostasis. Activation of TGR5 acts as a target for the treatment of obesity, diabetes and metabolic syndromes⁹. TGR5 is expressed in liver, lung, intestine, placenta, gallbladder, ovary, macrophages, monocytes and brown adipose tissue^{10,11}. TGR5 is also known as BA receptor, since it can be activated by BAs including cholic acid (CA), chenodeoxycholic acid (CDCA), deoxycholic acid (DCA) and lithocholic acid (LCA)¹². TGR5 agonist activates adenylyl cyclase cAMP signaling pathways and protein kinase-A pathway leads to the regulation of its target gene expression¹³. Previous reports on TGR5 suggest that activated TGR5 by BAs improved insulin sensitivity and glucose tolerance¹⁴.

BAs are potent signal molecules that exert genomic and non-genomic effects by the activation of nuclear hormone receptor FXR and G-protein coupled receptor TGR5. The two bile acid activated receptors (TGR5 and FXR) play a crucial role in targeting diabetes and metabolic disorders^{15,16,17}. Recently, 6 α -ethyl-3 α , 7 α , 23-trihydroxy-24-nor-5 β -cholan-23-sulfate sodium salt (INT-767) identified as dual FXR/TGR5 agonist. INT-767 is a novel, selective and first potent agonist that activate both BA receptors, including FXR (EC₅₀=0.033 μ M) and TGR5 (EC₅₀=0.67 μ M)¹⁸. Recent reports indicate that increased insulin sensitivity together with repression of the hepatic BA synthesis can be achieved by the treatment of INT-767. However,

the dual agonist INT-767, provide synergistic effects in the treatment of diabetes, obesity and metabolic disorders¹⁹.

Based on the significance, computational studies were performed to identify novel potent dual agonists of FXR/TGR5. This could be achieved through the combined method of e-pharmacophore model generation; pharmacophore-based virtual screening and free energy calculations. Molecular docking of INT-767 with BA receptors was performed to gain insights into the binding mode. Cross docking was carried out to find best suitable dual agonists among the screened compounds. Comparison study was performed for FXR-ligands and TGR5-ligands complexes using molecular dynamics simulations. Further, Density functional theory and ADME properties calculations were carried out to determine the electronic and drug-like properties of the compounds. Overall, the results of the present study expected to be useful in designing of novel dual agonists of FXR and TGR5.

Materials and methods

Protein preparation

Two different bile acid receptors including FXR and TGR5 have been used for the development of e-pharmacophore models. The crystal structure of the dimeric human FXR complexed with OMM (PDB ID: 3OMM) and our previously generated homology model of TGR5²⁰ was obtained for the generation of e-pharmacophore model. All structures were prepared using a multi-step process through *Protein Preparation Wizard* implemented in Schrödinger, LLC, New York, NY, USA, 2014. Crystallographic water molecules that present 5Å away from the ligand were removed and polar hydrogen atoms were added. Right bond orders, charges and atom types were assigned and side chains that are not involved in the formation of salt bridges were neutralized. Optimized Potentials for Liquid Simulations (OPLS)-2005 force field with an implicit solvation model was used for energy minimization. Optimization of hydrogen-bonding network, rotation of hydroxyl and thiol hydrogen atoms and generation of protonation and tautomerization states of His residues and Chi 'flip' assignments for Asn, Gln and His residues were achieved using protassign script. Further, restrained minimization was carried out until the average root mean square deviation (RMSD) of the non-hydrogen atoms reached 0.3Å.

Grid generation and ligand preparation

Ligand binding site for FXR was defined by generating the grid around the co-crystallized ligand location in the 3OMM structure. The grid was generated using the *Receptor*

Grid Generation panel with the default options. The sufficient large grid size with all active site residues identified experimentally by analyzing the protein-ligand interactions was chosen. According to our previous theoretical study²⁰, it was observed that the binding site of TGR5 was formed by active site residues including Ser21, Asn76, Tyr89, Asn93, Ser157, Trp237, Tyr240 and Ser270. Thus, the grid was generated at the centroid point of the active site for consistency. The well-known dual agonist of FXR/TGR5, namely, INT-767 was prepared using LigPrep module²¹ of Schrödinger with the consideration of proper ionization, tautomers, ring conformations and stereochemistries for further successful processing.

Induced Fit Docking

The protein structures of human FXR (3OMM) and human TGR5 were applied with the induced fit docking (IFD) method²² in the Schrödinger software suite. The prepared agonist INT-767 was docked into the active site of both proteins using standard protocols. Initially, ligand was docked to the rigid proteins using a softened potential in the Glide program with the van der Waals radii scaling of 0.7Å. Maximum of 20 poses per ligand were retained and used to sample the protein plasticity. Residues with at least one atom located within 5.0Å of each corresponding 20 ligand poses were subjected to a conformational search and minimization. During this process, residues occur outside the zone were fixed. The retained 20 ligand poses after minimization was redocked by Glide XP (extra precision) using default parameters. The binding affinity of the compound was reported in the Glide score. The more negative Glide score is more favorable in binding.

Generation of Energy-optimized pharmacophore model

The docking results of two different complexes, including FXR_{INT-767} and TGR5_{INT-767} were used for the generation of energy-optimized pharmacophore (e-pharmacophore) hypotheses for each complex using e-pharmacophore script available in Schrödinger script center. e-pharmacophore method combines the aspects of structure and ligand based approaches through the generation of energetically optimized pharmacophore. The energy-optimized pharmacophore model was investigated to screen millions of compounds^{23,24}. The docking poses of two protein-ligand complexes (FXR_{INT-767} and TGR5_{INT-767}) obtained from IFD were given as input to generate pharmacophore sites. Phase module implemented in Schrödinger was used for the generation of six built-in types of pharmacophore sites including hydrogen bond acceptor (A), hydrogen bond donor (D), hydrophobic region (H), negatively charged group (N), positively

charged group (P) and aromatic ring (R). The pharmacophore hypothesis was selected based on the ranking and quantification process. Finally, the two constructed e-pharmacophore models were used as a query to search chemical databases to retrieve compounds with novel and desired chemical features.

Pharmacophore-based virtual screening

Two constructed pharmacophore hypotheses such as AAN (TGR5_{INT-767}) and ADHN (FXR_{INT-767}), representing the chemical features of dual agonist INT-767 was obtained. Pharmacophore based screening was performed against ChemBridge database with ~520000 compounds to retrieve dual agonists of FXR and TGR5 with desired chemical features. Compounds from ChemBridge database were required to match a minimum of 3 or 4 sites on each generated hypothesis. The final hits from screening were ranked in order of Phase fitness score, a measure of how well the ligands matches the chemical features of pharmacophore sites based on vector alignments, volume terms and RMSD site matching. The molecules selected based on best fitness score were subjected to structure based virtual screening.

Structure based virtual screening

Multi-step structure based virtual screening was carried out using screened compounds obtained from pharmacophore screening. Glide²⁵ program was used to perform structure based virtual screening by three steps. In the first step, high-throughput virtual screening (HTVS) was carried out with default settings. Screened hits from HTVS were used in the second step, standard precision (SP) mode. Finally, the hits from SP were docked using extra precision (XP) mode of Glide to refine good ligand poses. Semi-flexible docking protocols were used for docking simulations. The Glide XP docked compounds from each protein was employed for further enrichment calculations.

Guner-Henry (GH) scoring method

The energy-based pharmacophore model employed for the high-throughput virtual screening and docking was validated using enrichment analysis. e-pharmacophore based virtual screening was again performed using database containing actives and decoy molecules in order to validate the reliability of two models (FXR_{INT-767} and TGR5_{INT-767}). The decoy set consists of 1000 drug-like molecules with an average molecular weight of 400 Daltons were downloaded from Schrodinger website (http://www.schrodinger.com/glide_decoy_set). A decoy set consists of 1045 molecules was used for FXR_{INT-767} complex generated e-pharmacophore screening. Of

these 1045 molecules, 45 molecules were known to be actives on the basis of high-throughput virtual screening results. In case of TGR5_{INT-767} complex generated e-pharmacophore model, the database containing 1022 molecules were used. Out of 1022 molecules, 22 molecules were known to be agonists of TGR5 with good docking scores. GH scoring method was successfully applied to quantify model selectivity. Furthermore, the hits retrieved from XP mode of Glide were investigated through cross docking. In cross docking, the compounds docked with TGR5 and FXR were cross docked with FXR and TGR5, respectively. Furthermore, IFD was carried out for the selected hits to produce reliable and comparable results with the well-known agonist.

Prime MM/GBSA

The top ranked poses of each dual agonist were rescored by binding free energy calculations. Prime/MM-GBSA method^{26, 27} was used for the prediction of binding free energy (ΔG_{bind}) for a set of ligands to the receptor. In the present study, binding free energy was calculated for ligands with both the proteins (TGR5 and FXR) using the following equation²⁸:

$$\Delta G_{\text{bind}} = \Delta E_{\text{MM}} + \Delta G_{\text{solv}} + \Delta G_{\text{SA}}$$

$$\Delta E = E_{\text{complex}} - E_{\text{protein}} - E_{\text{ligand}}$$

Where, E_{MM} is the difference in energy between protein-ligand complex and the sum of the energies of apo protein and ligand. G_{solv} is the difference between GBSA solvation energy of protein-ligand complex and the sum of the corresponding energies for the protein and ligand. ΔG_{SA} is the difference between the surface area energy of protein-ligand complex and the sum of the corresponding energies for the protein and ligand. E_{complex} , E_{protein} , and E_{ligand} are the minimized energies of the protein-ligand complex, protein, and ligand, respectively.

ADME prediction

The identified best four hits from cross docking were further studied for their absorption, distribution, metabolism and excretion (ADME) properties using QikProp²⁹. Toxicity levels of the compounds were predicted using the percentage of their human oral absorption. Furthermore, Lipinski rule of five³⁰ was applied to check the drug like properties of selected hits. The Qikprop results can provide predicting properties of molecules with novel scaffolds as for analogs of well-known drugs.

Density functional theory calculations

Density functional theory (DFT) calculations were used to estimate the chemical reactivity of the compounds. The best four compounds retrieved from cross docking were used as

inputs for DFT calculations. All DFT calculations have been performed with Jaguar v8.3 implemented in Schrödinger. Hybrid DFT with Berke's three-parameter exchange potential and Lee-Yang-Parr correlation functional (B3LYP), using basis set 3-21G* level was employed for the complete geometry optimization of structures. Energy calculations were performed in an aqueous environment using PBF. Highest Occupied Molecular Orbitals (HOMO) and Lowest Unoccupied Molecular Orbitals (LUMO) were calculated.

Molecular dynamics in implicit solvent

Molecular dynamics (MD) simulations were employed to confirm the binding mode obtained through molecular docking studies and to investigate the stability and dynamic behaviors of the agonists. Thus, MD simulations were carried out for best four compounds bound to FXR using Desmond v3.7 package of Schrödinger. All the four systems were minimized with Optimized Potentials for Liquid Simulations-All Atom (OPLS-AA 2005) force field and solvated with TIP3P water solvent model. The 10Å buffered orthorhombic box was filled with water molecules to set an aqueous environment. The complexes were immersed in the orthorhombic box. Overlapping water molecules were deleted and the overall charge of the system was neutralized by adding 8 Na⁺ counter ions. The energy of the systems was minimized up to a maximum of 5000 steps using the steepest descent method until a gradient threshold of 25 kcal/mol was reached. After energy minimization, MD simulations were carried out for four complexes in the NPT ensemble with the Nose-Hoover temperature coupling (300K) and the Martyna-Tobias-Klein pressure coupling (1 bar). Electrostatic interactions were calculated using Particle Mesh-Ewald summation scheme for long-range electrostatics. SETTLE algorithm³¹ was used to constrain the geometry of all covalent bonds containing water molecules. All the four FXR-agonist complexes were simulated for a time period of 10 ns.

Molecular dynamics in lipid bilayer

Molecular dynamics simulations were carried out in the membrane environment for the best four compounds bound with TGR5. In the system builder process of Desmond, minimization was carried out with OPLS-AA 2005 force field. POPC (1-palmitoyl-2-oleoyl-sn-glycero-3-phosphatidylcholine) lipid bilayer was used to construct 10Å buffered orthorhombic systems with periodic boundary conditions. The four TGR5-agonist complexes embedded in a POPC lipid bilayer were surrounded by explicit TIP3P water model. About 10 Cl⁻ counter ions were replaced water molecules in order to neutralize the system. The salt concentration of the

system was set to 0.15M Na⁺/Cl⁻. The simulation was carried out with periodic boundary conditions. In simulation process, the same protocol mentioned under Molecular dynamics in implicit solvent was followed. Before each dynamics, a default Desmond membrane protein relaxation protocol was applied. The MD simulation coordinates of all the systems were saved at 1.2 ps interval for further analyses.

***In vitro* studies**

Compounds

The best compound from e-pharmacophore based screening was selected for further *in vitro* studies based on the docking score, binding mode, interaction pattern and MD simulation analysis. The best compound ChemBridge_9149693 was purchased from ChemBridge (Hit2Lead) online chemical store (<https://www.hit2lead.com>) and dissolved in DMSO. The potency of compound was tested using insulin secreting pancreatic β -cell line MIN-6.

Cell culture and reagents

The insulin secreting pancreatic β -cell line MIN-6 was procured from National Centre for Cell Science (NCCS), Pune, India. The cells were cultured in Dulbecco's modified eagle's medium (DMEM) containing 25 mM glucose supplemented with 10% fetal bovine serum, L-glutamine, sodium carbonate, 2.5 mM 2-mercaptoethanol, 100 U/ml penicillin-streptomycin and incubated 37°C in 5% CO₂. Uric acid solution for cell treatments was prepared in the prewarmed cell culture medium (Ultrapure, Sigma; 1-15 mg/dL) and passed through a 20 μ m sterile filter.

Effect of compound on uric acid-induced cytotoxicity of MIN-6 cells

The MIN-6 cells were seeded in 96 well plates at a concentration of 1×10^5 cells per well. After 24 h, cells were washed twice with 100 μ l of serum-free medium and starved for an hour at 37°C. After starvation, cells were treated with different concentrations of ChemBridge_9149693 (1 μ g- 50 μ g/ml) for 24 h at 37°C.

Assessment of cell viability

The viability of the cells was assessed by the reduction of MTT (3-(4,5-dimethylthiazol-2-yl)-2,5-diphenyltetrazolium bromide) to formazan as described previously³². At the end of the treatment period, cells in each well were added 20 μ l of MTT (5mg/ml) and incubated for 4 h at 37°C in a CO₂ incubator. After removing the medium containing MTT, 200 μ l of phosphate buffered saline (PBS) was added to each well. The crystals were then dissolved by adding 100 μ l of DMSO. Spectrophotometrical absorbance of the purple blue formazan dye was measured in a

micro-plate reader at 570 nm (Bio-Rad 680). The absorbance of untreated cells was considered as 100%. The results were determined by three independent experiments. Cytotoxicity was determined using Graphpad prism5 software. The 50% inhibitory concentration value (IC_{50}) of the compound was identified for treated cell line.

Measurement of intracellular reactive oxygen species (ROS)

Intracellular reactive oxygen species were detected by fluorescent spectrophotometry using a fluorescein-based dye, DCFH-CA. Briefly, after treatment, the cells were cultured with 10 μ M DCFH-DA for 30 min at 37°C. Then, the cells were washed with PBS and homogenized in 300 μ l of 0.1% Triton-X-100 (PBS, pH 7.4) through sonication. The homogenates were centrifuged and the supernatants were used for assay after incubation at 4°C for 10 min with excitation wavelength at 488 nm and emission wavelength at 510 nm³³.

Estimation of antioxidant enzymes

For the estimation of antioxidant enzymes including catalase (CAT) and glutathione peroxidase (GPx), cells were seeded (0.2×10^6 cells per well) in six-well culture plates. Uric acid was added and the cells were incubated for 1 h. Then, the cells were treated with ChemBrigde_9149693 for 1 hr at 37°C. Further, the medium was removed and replaced with fresh medium and incubated again for another 22 h. At the end of the incubation time, cells were collected by centrifugation. The cell pellet was resuspended in PBS and then sonicated. The clear lysate was used to estimate the antioxidant enzymes such as CAT and GPx, determined by the method of Sinha (1972)³⁴ and Rotruck et al (1973)³⁵, respectively.

Results and Discussion

Binding mode analysis of dual agonist with FXR and TGR5

Flexibility of protein may be the most challenging issue in molecular docking due to the large size and degrees of freedom of protein³⁶. IFD protocol that considers protein flexibility was employed to predict the binding modes of FXR and TGR5. The dual agonist (INT-767) of FXR and TGR5 was docked into the binding site of both the receptors to determine the binding and interaction mode. The agonist showed stable interactions with both the proteins. The binding mode of INT-767 with FXR and TGR5 are shown in Figure 1. From the docking results of FXR, it was observed that eight amino acid residues such as Arg268, Met294, Asn297, His298, Arg335, Ser336, Ser359 and Tyr373 were seen as key players in the binding of INT-767. Total of twelve hydrogen bonding interactions were predicted for FXR_{INT-767} complex with the glide score

of -12.046 kcal/mol. Among these hydrogen bonds, five amino acids such as Arg268, Arg335, Ser336, Ser359 and Tyr373 were directly interacted with the compound. The amine group of the backbone of amino acid Arg268 ($\text{NH}\cdots\text{O}=\text{C}$, bond length=1.93Å) formed hydrogen bonding interaction with carboxyl group of INT-767. The amine group of Arg335 ($\text{NH}\cdots\text{O}-\text{S}-\text{O}$, bond length=2.40Å), ($\text{NH}_2\cdots\text{O}-\text{S}-\text{O}$, bond length=1.91Å) formed two hydrogen bonds with sulfate group of the compound, whereas hydroxyl group of Ser336 ($\text{HO}\cdots\text{HO}$, bond length=2.33Å) and Ser359 ($\text{HO}\cdots\text{HO}$, bond length=1.76Å) formed hydrogen bond with the hydroxyl group attached with INT-767. Additionally, two water mediated hydrogen bonding interactions ($\text{O}_2\text{H}\cdots\text{O}-\text{S}-\text{O}$, bond length=2.05Å) and ($\text{O}_2\text{H}\cdots\text{O}-\text{S}-\text{O}$, bond length=2.03Å) were noticed with sulfate group of the compound. Four protein-water interactions such as Arg268 ($\text{NH}\cdots\text{O}_2\text{H}$, bond length=1.83Å), Met294 ($\text{C}=\text{O}\cdots\text{H}_2\text{O}$, bond length=1.84Å), Asn297 ($\text{NH}\cdots\text{O}_2\text{H}$, bond length=1.83Å) and His298 ($\text{C}=\text{O}\cdots\text{H}_2\text{O}$, bond length=2.24Å). The agonist INT-767 was adjacent to some hydrophobic residues of protein, including Ile273, Ile277, Ile290, Leu291, Ala295, Val301, Met332, Ile339, Ile356, Ile361, Met369, Tyr373 and Trp458.

The dual agonist INT-767 was successfully docked into the binding site of TGR5 and possessed the docking score of -12.207 kcal/mol. The receptor-agonist interaction was predicted through the formation of five hydrogen bonds. The five key amino acids of TGR5 including Ser21, Tyr89, Trp237, Tyr240, and Ser270 formed hydrogen bonding interactions with the agonist. The hydrogen atom from the hydroxyl group of INT-767 was interacting with Ser21 ($\text{HO}\cdots\text{HO}$, bond length =2.03Å) and Ser270 ($\text{HO}\cdots\text{HO}$, bond length=2.06Å), forming hydrogen bonds. Sulfate ion present in INT-767 established hydrogen bonds with Tyr89 ($\text{HO}\cdots\text{O}-\text{S}-\text{O}$, bond length=1.78Å), Trp237 ($\text{NH}\cdots\text{O}=\text{S}$, bond length=2.45Å) and Tyr240 ($\text{OH}\cdots\text{O}-\text{S}-\text{O}$, bond length=1.76Å). The compound INT-767 was also adjacent to some hydrophobic residues of binding site, including Ala17, Leu18, Leu24, Ala25, Leu68, Pro69, Pro72, Pro92, Phe96, Leu97, Trp75, Leu263 and Leu266. Formation of hydrogen bonds between TGR5 and INT-767 was associated with only polar amino acids. Molecular docking results showed a good correlation with the experimentally determined activity of INT-767. Furthermore, the hydrogen bond interactions predicted through molecular docking were responsible for the experimental high agonistic activity toward TGR5 receptor. Overall, the results confirmed that the key amino acids involved in the binding of INT-767 in the active site of two receptors were entirely different that may helpful in the development of different dual agonists.

e-pharmacophore model and pharmacophore-based screening

Identification and development of new ligands with high binding affinity towards target protein is the major aim of drug design. Pharmacophore modeling was reported to be a very useful model to achieve this goal³⁷. In the present study, the validated docked complexes of FXR_{INT-767} and TGR5_{INT-767} were selected to develop a pharmacophore model. e-pharmacophores were generated by mapping the energetic values generated by a scoring function of Glide XP onto the atom center. Four featured pharmacophore hypothesis (ADHN) consist of one acceptor (A), one donor (D), one hydrophobic region (H) and one negatively charged group (N) was generated for FXR_{INT-767} complex. In case of TGR5_{INT-767}, three featured pharmacophore hypothesis (AAN) was obtained with two acceptors (A) and one negatively charged group (N). These two pharmacophore models were selected based on the scoring function. The two hypothetical pharmacophore models ADHN and AAN, representing the chemical features of dual FXR and TGR5 agonist (INT-767) are shown in Figure 2. Virtual screening against chemical databases helps to determine the capability of generated pharmacophore model in the identification of active and inactive compounds³⁸. In the current study, the generated pharmacophore models were used as query to search against ChemBridge database to retrieve compounds that match pharmacophore features of the model. The molecules possessed fitness scores higher than 1.200 were subjected to high-throughput virtual screening against FXR and TGR5 separately.

Structure based virtual screening

The hits selected based on the fitness score were further used as input for structure based virtual screening. The compounds retrieved from the pharmacophore model ADHN were subjected to HTVS using FXR as receptor. Likewise, molecules that fit with hypothetical pharmacophore AAN were docked into the binding site of TGR5. Through the first step HTVS, the potential ligands that able to bind with FXR and TGR5 were retrieved. Next, Glide SP was used for further refinement of the screened compounds through HTVS. The ligands retrieved from the results of SP were used for the more precise Glide XP docking protocol. Finally, 35 ligands that effectively interact with the binding site of FXR as well as 22 ligands that effectively bind to the active site residues of TGR5 were retrieved through the docking procedure. For further validation, the screened compounds combined into a single file and cross docking was performed with both the receptors using XP docking mode. In this step, 35 compounds docked

into the binding site of TGR5 and 22 compounds docked to FXR. Using this approach, best four compounds that able to bind to the active site of both BA receptors were selected based on the glide score, glide energy, binding conformation and stable interaction pattern. Furthermore, IFD protocol was applied in order to determine the correlation between the identified four hits and well-known dual agonist INT-767. From the IFD results, it was confirmed that all four identified hits were very close to the binding mode of the dual agonist INT-767. The flowchart of ligand (e-pharmacophore) and structure based virtual screening is shown in Figure 3.

Enrichment calculations

The GH analysis was carried out by computing the enrichment factors (EF), goodness of hit (GH) and other statistical values such as total number of active compounds in the database (A), total number of compounds in the database (D), total number of screened compounds using pharmacophore model (Ht), total number of active molecules screened (Ha), false negatives and false positives. These statistical values calculated for both e-pharmacophore models $FXR_{INT-767}$ and $TGR5_{INT-767}$ are given in Table 1. The $FXR_{INT-767}$ e-pharmacophore model scored an enrichment factor of 17.97 and a GH score of 0.6918. In case of $TGR5_{INT-767}$ e-pharmacophore model, the computed enrichment factor and GH score was found to be 21.21 and 0.5940, respectively. The enrichment study results clearly indicated the good quality and reliability of the generated two e-pharmacophore models. Also, the study suggested that the two hypotheses have the ability to discriminate and separate the actives from inactives. Thus, the active compounds retrieved using these two e-pharmacophore models helps in the development of new agonists of FXR and TGR5.

Binding mode analysis of potent compounds with FXR

The docking results of the best four compounds retrieved from ChemBridge database with ChemBridge ID of 9149693 (5-oxo-5-[(3-{{(tetrahydro-2-furanylmethyl)amino}carbonyl}phenyl) amino] pentanoic acid), 9135270 (4-oxo-4-[(3-{{(tetrahydro-2-furanylmethyl)amino}carbonyl}phenyl)amino]butanoic acid), 7725166 (5-oxo-5-[(4-{{(3-pyridinylmethyl)amino}carbonyl}phenyl)amino]pentanoic acid) and 9042904 (4-{{(1,3-benzodioxol-5-ylamino)carbonyl}amino}methyl)benzoic acid) are shown in Table 2. These compounds screened on the basis of the shape and pharmacophoric features of INT-767. Unexpectedly, all four hit compounds had very similar chemical structures. The binding mode analysis of each potent compound was discussed detail to understand the binding affinity and

interactive mode of the compound to the binding site of BA receptors including FXR and TGR5. ChemBridge_9149693 docked into the binding site of FXR and exhibited a docking score of -12.834 kcal/mol. The compound showed two protein-ligand interactions (Arg335, Tyr373), one water-protein interaction (Met294-H₂O) and two water mediated interactions. The negatively ionizable charge (N) interacted with the side chain of Arg335 (NH₂...O-C, bond length=2.01Å) and two water molecules (O₂H...O=C, bond length, 2.62Å), (O₂H...O=C, bond length, 1.81Å). The acceptor site (A) of the pharmacophore formed hydrogen bond interaction with the side chain of Tyr373 (OH...O=C, bond length, 1.75Å).

The binding conformation of ChemBridge_9135270 showed that amine group of the compound established a hydrogen bond with hydroxyl group of the side chain of Ser336 (HO...HN, bond length, 2.50Å). Arg335 showed one salt bridge (NH₂...O-C, distance, 4.88Å) and one hydrogen bond interaction (NH...O=C, bond length, 1.87Å) with the amine group of the compound. The carboxyl group of ChemBridge_9135270 formed a hydrogen bond interaction with hydroxyl group of Tyr373. Like other compounds, ChemBridge_9135270 also established two water mediated and two protein-water interactions. In case of ChemBridge_7725166, the docking results showed that the oxygen atom of the compound established hydrogen bond interaction with the amine group of Arg335 (NH₂...O-C, bond length, 1.75Å). The carboxyl group of the compound formed hydrogen bond with hydroxyl group of Tyr373 (OH...O=C, bond length, 1.78Å). ChemBridge_7725166 also showed two water mediated interactions (O₂H...O=C, bond length, 1.77Å), (O₂H...O=C, bond length, 2.1Å) and two protein-water interaction with Met294 (C=O...H₂O, bond length, 1.79Å) and Arg268 (NH...O₂H, bond length, 2.06Å). The π - π stacking interaction was also observed between the compound and Phe333 with the distance of 5.07Å.

Like other compounds, ChemBridge_9042904 also showed hydrogen bond interactions with a side chain of Arg335 and Ser336. Negative site was interacted with the amine group of Arg335 (NH...O=C, bond length, 1.76Å) and two water molecules. In addition, Arg335 was formed a salt bridge with the compound with the distance of 3.30Å. Interestingly, the aromatic-aromatic (π - π) stack pairing was also observed between the compound and Phe333 with the distance of 4.78 Å. The side chain of Ser336 (HO...HN, bond length, 2.18Å), (HO...HN, bond length, 1.84Å) formed two hydrogen bond interactions with the amine groups present in the compound. From the docking conformation, it was observed that all four compounds showed a

similar binding mode with the active site residues of FXR and established a similar water mediated interactions and hydrophobic interactions with some of the amino acids. Overall, the four compounds were positioned in the same orientation and shared a similar binding pattern as to that of co-crystallized ligand. The chemical structures and interaction modes between the four identified compounds and FXR generated using ligand interaction diagram in Schrödinger are illustrated in Figure 4. The docking results revealed that two out of four compounds were involved in π - π stacking interactions with the amino acid Phe333. The hydrophobic contact and water mediated interactions with active site residues of FXR play a pivotal role in the binding of ligands. The prime MM/GBSA rescoring showed better correlation with the IFD docking calculations. The results of MM/GBSA calculations indicated that the four leads ChemBridge_9149693, ChemBridge_9135270, ChemBridge_7725166 and ChemBridge_9042904 bound strongly to the FXR protein.

Binding mode analysis of potent compounds with TGR5

ChemBridge_9149693 exhibited a high docking score of -12.403 and showed four hydrogen bonding interactions with Asn93, Glu169, Trp237 and Tyr240. The negative site of the pharmacophore interacted with two amino acids Glu169 and Tyr240. Specifically, carboxyl group of the compound established a hydrogen bond interaction with hydroxyl H atom of Tyr240 ($\text{OH}\cdots\text{O}=\text{C}$, bond length, 1.94Å). The oxygen atom of the compound formed a hydrogen bond with hydroxyl H atom of the side chain of Glu169 ($\text{OH}\cdots\text{O}-\text{C}$, bond length, 1.74Å). Another hydrogen bond was formed between the amine group of ChemBridge_9149693 (NH) and carboxyl group of Asn93 ($\text{C}=\text{O}$) with the distance of 1.98Å. The NH group of Trp237 favoured hydrogen bonding interaction with the $\text{C}=\text{O}$ group of ChemBridge_9149693. The top ranked pose obtained for ChemBridge_9135270 showed that the compound possessed the docking score of -11.170kcal/mol and formed four hydrogen bonds with active site residues of TGR5, including Glu169 ($\text{OH}\cdots\text{O}-\text{C}$, bond length, 1.76Å), Tyr237 ($\text{OH}\cdots\text{O}=\text{C}$, bond length, 1.87Å), Tyr240 ($\text{NH}\cdots\text{O}=\text{C}$, bond length, 1.85Å) and Leu266 ($\text{C}=\text{O}\cdots\text{HN}$, bond length, 2.15Å). Additionally, π - π stacking interaction was also noticed between the aromatic ring of ChemBridge_9135270 and aromatic ring of Phe96 with the distance of 3.89Å. The π - π interactions play a crucial role in the recognition of protein-ligand binding mechanism and stabilization of complexes.

The binding mode of ChemBridge_7725166 showed that the compound bound strongly to the receptor through four hydrogen bond interactions with Tyr89 ($\text{OH}\cdots\text{O}-\text{C}$, bond length,

1.94Å), Asn93 (NH₂...O-C, bond length, 2.20Å), Trp237 (NH...O=C, bond length, 1.84Å) and Ser270 (OH...N-C, bond length, 2.22Å). From the binding conformation of ChemBridge_9042904, it was observed that the compound possessed the docking score of -12.268 kcal/mol and established three hydrogen bond interactions and two π - π interaction with key residues of TGR5, including Tyr89, Phe96, Ser157 and Trp237. Among these residues, Ser157 (C=O...HN, bond length, 2.05Å), (C=O...HN, bond length, 1.93Å) and Trp237 (NH...O=C, bond length, 1.88Å) established hydrogen bond interactions. Other two residues Tyr89 and Phe96 formed π - π stacking interactions with the distance of 5.19Å and 5.01Å, respectively. Specifically, hydrophobic interactions were observed for all four compounds with some of the active site residues. In case of TGR5 also, the entire four compounds shared similar orientation and binding mode. The binding mode of the compounds into the active site of TGR5 is displayed in Figure 5.

The results revealed that most of the interacted amino acids are conserved in all the analyzed interactions. In particular, Phe96 plays an importance role in complex involving π - π stacking interactions with ChemBridge_9135270 and ChemBridge_9042904. From the results, it was demonstrated that hydrophobic and π - π stacking interactions were playing an important role in the binding of ligands into the active site of receptor. For further validation, MM/GBSA approach was used to calculate the binding free energy for each complex in order to evaluate affinities of the selected four agonists to both FXR and TGR5. The docking results, including docking score, glide emodel, glide energy, hydrogen, hydrophobic interactions and binding free energy of top four leads with TGR5 and FXR are tabulated in Table 2. From the comparison of docking and binding free energy calculations, it was observed that there was a good correlation between them.

ADME prediction

Pharmacologically important properties were predicted using Qikprop for the best four leads. The calculated properties such as molecular weight, aqueous solubility (log S), predicted octanol/water partition coefficient (QPlogPo/w), skin permeability (QPlogKp), percentatge of human oral absorption and Lipinski rule of five are tabulated in Table 3. According to the ADME prediction results, it was found that pharmacokinetic properties of all identified hits were in the desirable range defined for human use. Thus, four leads (ChemBridge_9149693, ChemBridge_9135270, ChemBridge_7725166 and ChemBridge_9042904) indicate their

potential as drug like molecules with low toxicity and suitable for further development of anti-diabetic drugs.

DFT analysis

Electronic properties of the four best hits were characterized using frontier orbital energies (HOMO and LUMO). LUMO is directly associated with the electron affinity and system's tendency to accept electron density. HOMO is directly associated with the ionization potential. The HOMO and LUMO distributions, energies and energy gaps were calculated for the four hits were computed. Chemical stability of a molecule can be determined by the energy gap between HOMO and LUMO. A small gap between the two frontier orbitals implies high reactivity, low stability, implicitly high polarizability of the compound³⁹. According to the outcome of DFT calculations, the difference between the HOMO and LUMO values were small. Likewise, the HOMO and LUMO energies were small, ranging between -0.198 to -0.191 and -0.04 and -0.01 eV, respectively, indicates the fragile nature of bound electrons. The energy gap between the HOMO and LUMO energies (HLG) varies between 0.15 and 0.16 eV. Rapid electron transfer and exchange are equally possible by making the compounds very reactive due to small values of HOMO and LUMO. The calculated energies and energy gaps are tabulated in Table 4.

HOMO and LUMO distributions are plotted onto the surface of four hits are displayed in Figure 6. From the figure, it can be seen that the distribution of HOMO and LUMO energies are located in two distinct parts of the molecules. A well-defined separation in location is noticed from the figure. Analysis of HOMO maps of ChemBridge_9149693 illustrates that HOMO molecular orbitals are located on the carboxyl group (Pentanoic acid), indicates the existence of possible reactive sites. Interestingly, electrophilic attack takes place at the active site residues of FXR and TGR5. LUMO maps are located on the phenyl, carbonyl and amino group of the compound. In case of ChemBridge_9135270, the HOMO orbitals are located on the carboxyl and amino group, whereas LUMO are located on the carbonyl, phenyl and amino group of the compound. However, compare to ChemBridge_9149693, the HOMO energy level was lower while the LUMO energy level was higher. The energy gap between the HOMO and LUMO of ChemBridge_9135270 was 0.15 eV. The frontier orbital energies of ChemBridge_7725166 and ChemBridge_9042904 are plotted in Figure 6c and 6d. The HOMO distributions are observed on the carboxyl group, while LUMO observed on the carbonyl, phenyl and amino group of

ChemBridge_7725166. In case of ChemBridge_9042904, HOMO are distributed on the carboxyl group attached to benzoic acid, whereas LUMO are distributed on the 4-((1, 3-benzodioxol-5-yl amino) group. Compare to other three compounds, the increased HOMO and decreased LUMO energy levels were observed. The H-L gap of ChemBridge_9042904 was higher compared to other three compounds (0.187 eV). The distributions of HOMO and LUMO onto the surface of identified compounds indicate that the compounds are highly reactive in nature. The DFT calculations provide additional details regarding the agonistic activity of the identified hits. The comparison of docking and DFT results, revealed that the carboxyl group of the four compounds involved in the formation of important hydrogen bond interactions (hinge interaction) with the active site residues of FXR and TGR5.

MD analysis of FXR_{agonist} complexes in implicit solvent environment

In order to explore the detailed interactions between the FXR receptor and four agonists, MD simulation was carried out. The trajectories generated using Desmond after the simulation time of 10 ns was used for the analysis. The backbone root mean square deviation (RMSD) and root mean square fluctuation (RMSF) of all four complexes were analyzed. The backbone RMSD of each FXR_{agonist} complexes is outlined in the Figure 7. All four protein-ligand complexes showed stable and low RMSD values, indicating the stability of complexes during the simulation period of 10 ns. However, all complexes reached initial equilibrium at around 2 ns and attained stable conformation with the RMSD near 3.2 to 3.5 Å. Also, all four complexes showed very less deviations from the initial structure. Thus, the RMSD plot confirmed the stability of FXR_{agonist} complexes. The fluctuations with backbone atoms with respect to TGR5 residues are displayed in Figure 8. From the RMSF plot, it can be seen that most of the residues in TGR5 are stable and very few residues show less fluctuations. In particular, the residues involved in the formation of hydrogen bond interactions showed very less fluctuations. Furthermore, all four agonists formed stable hydrogen bond interactions with Met294, Arg268, Asn297, Phe333, Arg335, Ser336 and Tyr373 of FXR receptor. The constant hydrogen bond interactions throughout the simulation period of 10 ns are displayed in Figure 9. The hydrophobic interactions formed between the receptor and agonists remains same and stable throughout the MD simulation period of 10 ns. Thus, MD simulation results of FXR_{agonist} complexes indicating the stability of all the complexes.

MD analysis of TGR5_{agonist} complexes in lipid bilayer environment

The RMSD of backbone atoms from their initial configuration as a function of simulation time of 10 ns for the investigated four TGR5_{agonist} complexes are represented in Figure 10. From the figure, it was noticed that the obtained MD trajectory was stable and equilibrated at around 6 ns. The protein and ligands were found to be relatively stable during the simulation period of 10 ns. It was observed that the backbone RMSD was increased in the beginning and after 6 ns it became almost constant for the rest of the MD simulation. In case of TGR5-ChemBridge_9149693 complex, small deviations are occur when compared with the other three complexes. The compound was stabilized around 8 ns and maintained the stability throughout the simulation period of 10 ns. Also, the RMSD values lies within 6Å for all the four systems indicating the conformational stabilities of the protein structures upon binding of agonists. The backbone RMSF of TGR5 residues in four TGR5_{agonist} complexes are represented in Figure 11. From the figure, it was observed that the RMS fluctuations are very low and most of the residues are free from the fluctuations. In particular, the active site residues involved in the formation of hydrogen bonding interactions such as Tyr89, Asn93, Phe96, Ser157, Glu169, Trp237, Tyr240, Leu266 and Ser270 are found to be stable and very fewer fluctuations are observed with these residues. Also, the residues responsible for the formation of hydrophobic, hydrogen bonding and μ - μ stacking interactions are found to be stable throughout the MD simulation of 10 ns. The constant hydrogen bonding interactions of four complexes throughout the MD simulation of 10 ns are represented in Figure 12.

In vitro assays

Cell viability

A cytotoxicity and IC₅₀ value of the ChemBrigde_9149693 was tested against MIN-6 pancreatic β -cell lines. Effects of ChemBrigde_9149693 at different concentrations on uric acid-induced cytotoxicity of MIN-6 cells are displayed in Figure 13. The potent compound ChemBrigde_9149693 exhibited IC₅₀ value in the low micromolar range (slightly less than 10 μ g). The exact IC₅₀ value of ChemBrigde_9149693 on uric acid induced MIN-6 cell lines was found to be 9.89 μ g/ml. The treatment with ChemBrigde_9149693 up to 50 μ g/ml dose at 37°C, did not induce cytotoxicity and cell viability was found to be more than 80%. Therefore, all further studies were carried out using this IC₅₀ concentration. The results revealed that the

compound at different concentration was found to have significant protection against uric acid induced cytotoxicity.

Intracellular ROS

Intracellular ROS generation was increased up to three fold after uric acid induction and it was obviously suppressed by the treatment of ChemBrigde_9149693 ($IC_{50} = 9.89 \mu\text{g/ml}$). The suppression of intracellular ROS by ChemBrigde_9149693 was compared with the control and uric acid induced group and represented in Figure 14.

Effect of the compound on antioxidant enzymes

The effect of ChemBrigde_9149693 on the activities of CAT and GPx in uric acid-induced insulin secreting pancreatic β -cell line MIN-6 was assessed. The level of antioxidant enzymes such as CAT and GPx before and after treatment of ChemBrigde_9149693 are represented in a bar diagram in Figure 15 and 16, respectively. From figure 15, it can be seen that the level of CAT is decreased after the induction of uric acid and it is reversed by the treatment of ChemBrigde_9149693, which is compared with the control group. Likewise, in figure 16, it was observed that the level of antioxidant enzyme GPx was also decreased in uric acid-induced group and it is reversed with the treatment of the potent compound.

Conclusion

The activation of FXR and TGR5 has increasingly gained attention for anti-diabetic drug discovery. In this study, computational approaches were used for the identification of potent compounds that can able to activate both BA receptors. From the results, it was concluded that all the protocols including pharmacophore hypotheses, docking, ADME toxicity prediction, DFT, binding free energy calculations and virtual screening were able to predict potent suitable dual inhibitors of FXR and TGR5. Analysis of docking and binding free energy calculations showed a better correlation between them. Furthermore, the binding mode and stability of the complexes were confirmed with the help of MD simulations. The e-pharmacophore based virtual screening supported by *in vitro* assays is an effective approach for the identification of novel drugs for the treatment of type II diabetes. The performed *in vitro* assays explained the potency of screened compound ChemBrigde_9149693 with anti-diabetic activity. Further studies are needed to check the activity of screened compound on FXR and TGR5. Overall, the results of the present study may provide insights into the development of novel effective dual agonists of FXR and TGR5.

Acknowledgement

Authors are grateful to thank the Department of Bioinformatics, Alagappa University, Karaikudi, India and UGC Innovative Scheme (No. F. 14-13/2013 (Inno/ASIST) for the computational facilities provided for this work. Also, we thank Dr. V. I. Hairul Islam for his excellent support and help with the cell line work.

Conflict of interest

There is no conflict of interest

References

1. J. Wada and H. Makino, *Clin. Sci (Lond.)*, 2013, 124, 139-152.
2. D. Merk, M. Gabler, R. C. Gomez, D. Flesch, T. Hanke, A. Kaiser, C. Lamers C, O. Werz, G. Schneider and M. Schubert-Zsilavecz, *Bioorg. Med. Chem*, 2014, 22, 2447-2460.
3. J. Y. L. Chiang, *J. Lipid Res*, 2009, 50, 1955-1966.
4. S. Caron, C. Huaman Samanez, H. Dehondt, M. Ploton, O. Briand, F. Lien, E. Dorchies, J. Dumont, C. Postic, B. Cariou, P. Lefebvre and B. Staels, *Mol. Cell. Biol*, 2013, 11, 2202-2211.
5. P. Lefebvre, B. Cariou, F. Lien, F. Kuipers and B. Staels, *Physiol. Rev*, 2009, 147-191.
6. L. Wang, X. Huang, S. Hu, X. Ma, S. Wang and S. Pang, *Chin. Med. J*, 2014, 127, 218-224.
7. T. Sindhu and P. Srinivasan, *J. Recept. Signal. Transduct. Res*, 2014, 34, 241-253.
8. M. Marinozzi, A. Carotti, R. Sardella, F. Buonerba, F. Ianni, B. Natalini, D. Passeri, G. Rizzo and R. Pellicciari, *Bioorg. Med. Chem*, 2013, 21, 3780-3789.
9. J. Zhu, M. Ning, C. Guo, L. Zhang, G. Pan, Y. Leng and J. Shen, *Eur. J. Med. Chem*, 2013, 69, 55-68.
10. S. Rajagopal, D. P. Kumar, S. Mahavadi, S. Bhattacharya, R. Zhou, C. U. Corvera, N. W. Bunnett, J. R. Grider and K. S. Murthy, *Am. J. Physiol. Gastrointest. Liver. Physiol*, 2013, 304, G527-535.
11. C. Thomas C, R. Pellicciari, M. Pruzanski, J. Auwerx and K. Schoonjans, *Nat. Rev. Drug. Discov*, 2008, 7, 678-693.
12. S. Fiorucci, A. Mencarelli, G. Palladino and S. Cipriani, *Trends. Pharmacol. Sci*, 2009, 30, 570-580.

13. M. Baptissart, A. Vega, S. Maqdasy, F. Caira, S. Baron, J. M. Lobaccaro and D. H. Volle, *Biochimie*, 2013, 95, 504-517.
14. M. Watanabe, S. M. Houten, C. Matakai, M. A. Christoffolete, B. W. Kin, H. Sato, N. Messaddeq, J. W. Harney, O. Ezaki, T. Kodama, K. Schoonjans, A. C. Biancom and J. Auwerx, *Nature*, 2006, 439, 484-489.
15. D. Schuster, P. Markt, U. Grienke, J. Mihaly-Bison, M. Binder, S. M. Noha, J. M. Rollinger, H. Stuppner, V. N. Bochkov and G. Wolber, *Bioorg. Med. Chem.*, 2011, 19, 7168-7180.
16. J. Fu, P. Si, M. Zheng, L. Chen, X. Shen, Y. Tang and W. Li, *Bioorg. Med. Chem. Lett.*, 2012, 22, 6848-6853.
17. R. Pellicciari, A. Gioiello, P. Sabbatini, F. Venturoni, R. Nuti, C. Colliva, G. Rizzo, L. Adorini, M. Pruzanski, A. Roda and A. Macchiarulo, *ACS Med. Chem. Lett.*, 2012, 3, 273-277.
18. A. Baghdasaryan, T. Claudel, J. Gumhold, D. Silbert, L. Adorini, A. Roda, S. Vecchiotti, F. J. Gonzalez, K. Schoonjans, M. Strazzabosco, P. Fickert, M. Trauner, *Hepatology*, 2011, 54, 1303-1312.
19. A. Roda, R. Pellicciari, A. Gioiello, F. Neri, C. Camborata, D. Passeri, F. De Franco, S. Spinozzi, C. Colliva, L. Adorini, M. Montagnani and R. Aldini, *J. Pharmacol. Exp. Ther.*, 2014, 350, 56-68.
20. T. Sindhu and P. Srinivasan, *RSC. Adv.*, 2015, 5, 14202-14213.
21. *LigPrep, version 2.9*, Schrödinger, LLC, New York, NY, 2014.
22. R. Farid, T. Day, R. A. Friesner and R. A. Pearlstein, *Bioorg. Med. Chem.*, 2006, 14, 3160-3173.
23. R. Palakurti, D. Sriram, P. Yogeewari and R. Vadrevu, *Mol. Inf.*, 2013, 32, 385-398.
24. B. R. Miller III and A. E. Roitberg, *J. Mol. Graph. Model.*, 2013, 45, 84-97.
25. *Glide, version 6.2*, Schrödinger, LLC, New York, NY, 2014.
26. *Prime, version 3.5*, Schrödinger, LLC, New York, NY, 2014.
27. H. Sun, Y. Li, M. Shen, S. Tian, L. Xu, P. Pan, Y. Guan and T. Hou, *Phys. Chem. Chem. Phys.*, 2014, 16, 22035-22045.
28. P. D. Lyne, M. L. Lamb and J. C. Saeh, *J. Med. Chem.*, 2006, 49, 4805-4808.

29. *QikProp, version 3.9*, Schrödinger, LLC, New York, NY, 2014.
30. C. A. Lipinski, F. Lombardo, B. W. Dominy and P. Feeney, *J. Adv. Drug Deliv. Rev*, 1997, 23, 3-25.
31. S. Miyamoto and P. A. Kollman, *J. Comput. Chem*, 1992, 13, 952-962.
32. H. Weichert, I. Blechschmidt, S. Schroder and H. Ambrosius, *Allerg. Immunol*, 1991, 37, 139-144.
33. J. F. Wang, T. R. Jerrells and J. J. Spitzer, *Free. Radical. Biol. Med*, 1996, 20, 533-542.
34. A. K. Sinha, *Anal. Biochem*, 1972, 47, 389-394.
35. J. T. Rotruck, A. L. Pope, H. E. Ganther, A. B. Swanson, D. G. Hafeman and W. G. Hoekstra, *Science*, 1973, 179, 588-590.
36. S. Y. Huang and X. Zou, *Int. J. Mol. Sci*, 2010, 11, 3016-3034.
37. S. Saxena, P. B. Devi, V. Soni, P. Yogeewari and D. Sriram, *J. Mol. Graph. Model*, 2014, 47, 37-43.
38. R. P. Gangwal, N. R. Das, K. Thanki, M. V. Damre, G. V. Dhoke, S. S. Sharma, S. Jain and A. T. Sangamwar, *J. Mol. Graph. Model*, 2014, 49, 18-24.
39. R. Curpan, S. Avram, R. Vianello and C. Bologna, *Bioorg. Med. Chem*, 2014, 22, 2461-2468.

Table 1: Statistical parameters obtained using decoy set validation for two generated e-pharmacophore models

Parameter	ADHN model	AAN model
Total number of molecules in the database (D)	1035	1022
Total number of actives in the database (A)	35	22
Total hits (Ht)	51	46
Active hits (Ha)	31	22
% Yield of actives [(Ha/Ht)*100]	60.78	47.82
% Ratio of actives [(Ha/A)*100]	88.57	100
Enrichment factor (E) (Ha*D)/(Ht*A)	17.97	21.21
False negatives (A-Ha)	4	0
False positives (Ht-Ha)	20	24
Goodness of hit score (GH) ^a	0.6918	0.5940

^a [(Ha/4HtA) (3A+Ht)) x (1 - ((Ht - Ha)/(D - A))] GH score of 0.6-0.8 indicates a very good model

Table 2: Induced fit docking and binding free energy calculation results of selected four active compounds

Compound	ChemBridge ID	H bond interactions	Hydrophobic interactions	Docking score	Glide energy	Glide Emodel	ΔG_{bind}
FXR _{agonists}							
1	9149693	Met294, Arg335, Tyr373	Ile273, Ile290, Leu291, Met332, Phe333, Ile339, Ile361, Met369, Met454, Leu455, Trp458, Trp473	-12.834	-53.698	-84.239	-98.359
2	9135270	Met294, Asn297, Arg335, Ser336, Tyr373	Ile273, Ile277, Leu291, Met332, Phe333, Ile339, Leu352, Ile356, Ile361, Met369, Met454, Phe447, Trp458, Trp473	-13.318	-60.931	-98.460	-100.732
3	7725166	Arg268, Met294, Asn297, Phe333, Arg335, Tyr373	Ile273, Ile277, Leu291, Met332, Ile339, Ile356, Ile361, Met369, Met454, Leu455, Trp458, Trp473	-12.897	-51.852	-80.140	-87.858
4	9042904	Met294, Asn297, Phe333, Arg335, Ser336	Ile273, Leu291, Ala295, Met332, Ile339, Ile361, Met369, Tyr373, Met454, Leu455, Trp458, Trp473	-15.332	-52.906	-82.108	-76.399
TGR5 _{agonists}							

1	9149693	Asn93, Glu169, Trp237, Tyr240	Leu68, Pro69, Pro72, Tyr89, Pro92, Phe96, Leu97, Phe138, Ala159, Phe161, Leu166, Val170, Leu174, Leu244, Leu263, Leu266	-12.403	-60.340	-97.402	-91.534
2	9135270	Phe96, Glu169, Trp237, Tyr240, Leu266	Leu68, Pro69, Pro72, Tyr89, Pro92, Leu97, Ala159, Leu166, Val170, Leu174, Leu244, Leu263	-11.170	-61.430	-95.595	-86.678
3	7725166	Tyr89, Asn93, Trp237, Ser270	Leu68, Pro69, Pro72, Pro92, Phe96, Leu97, Ala159, Phe161, Leu166, Val170, Leu174, Tyr240, Val241, Leu244, Leu266	-12.793	-61.639	-106.002	-81.740
4	9042904	Tyr89, Phe96, Ser157, Trp237	Leu68, Pro72, Pro92, Leu97, Phe138, Leu174, Tyr240, Leu263, Leu266	-12.268	-56.368	-89.698	-76.263

Table 3: ADME prediction results of best four hits identified through e-pharmacophore and structure based virtual screening

Compound	ChemBridge ID	Molecular weight	QPlogPo/W ^a	QPlogS ^b	QPlogKp ^c	Percentage of human oral absorption ^d	Rule of five ^e
1	9149693	334.371	1.814	-3.738	-3.710	66.583	0
2	9135270	320.344	1.475	-3.402	-3.805	64.600	0
3	7725166	341.366	1.934	-4.172	-3.947	60.370	0
4	9042904	314.297	1.712	-2.292	-3.226	65.871	0

^a Log of the predicted octanol/water partition co-efficient (acceptable range -2.0 to 6.5)

^b Log of the aqueous solubility; S in mol/L (acceptable range -6.5 to 0.5)

^c Predicted skin permeability (acceptable range -8.0 to -1.0)

^d Percentage of human oral absorption (<25% is poor and >80% is high)

^e Lipinski rule of five (maximum 4)

Table 4: Frontier orbital energies of the four identified agonists

Compound d	ChemBridge ID	HOMO (eV)	LUMO (eV)	HLG (eV)
1	9149693	-0.193	-0.043	0.150
2	9135270	-0.191	-0.041	0.150
3	7725166	-0.195	-0.035	0.160
4	9042904	-0.198	-0.010	0.187

Figure legends

Figure 1: Docked conformation of INT-767 into the active site of FXR (a) and TGR5 (b). The important active site residues in the binding pocket are represented by blue lines. Hydrogen bond interactions between the agonist and proteins are indicated by magenta dashed lines.

Figure 2: e-pharmacophore sites of FXR_{INT-767} (a) and TGR5_{INT-767} (b) along with the intersite distance.

Figure 3: Schematic representation of the overall work flow applied for lead identification based on e-pharmacophore based virtual screening.

Figure 4: Two-dimensional schematic representations of protein-ligand interactions between FXR and top four hits (a) ChemBridge_9149693 (b) ChemBridge_9135270 (c) ChemBridge_7725166 (d) ChemBridge_9042904 obtained from e-pharmacophore and structure based virtual screening.

Figure 5: Schematic two-dimensional diagrams of protein-ligand interactions between TGR5 and top four hits (a) ChemBridge_9149693 (b) ChemBridge_9135270 (c) ChemBridge_7725166 (d) ChemBridge_9042904.

Figure 6: Distribution of HOMO (left) and LUMO (right) of selected four hits (a, b) ChemBridge_9149693 (c, d) ChemBridge_9135270 (e, f) ChemBridge_7725166 and (g, h) ChemBridge_9042904.

Figure 7: The backbone RMSD of four FXR_{agonist} complexes over the simulation period of 10 ns.

Figure 8: The RMSF of four FXR_{agonist} complexes during the MD simulation period of 10 ns.

Figure 9: Total number of intermolecular hydrogen bonding interactions between four agonists in complex with FXR

Figure 10: The backbone RMSD of four TGR5_{agonist} complexes over the simulation period of 10 ns.

Figure 11: The RMSF of four TGR5_{agonist} complexes during the MD simulation period of 10 ns.

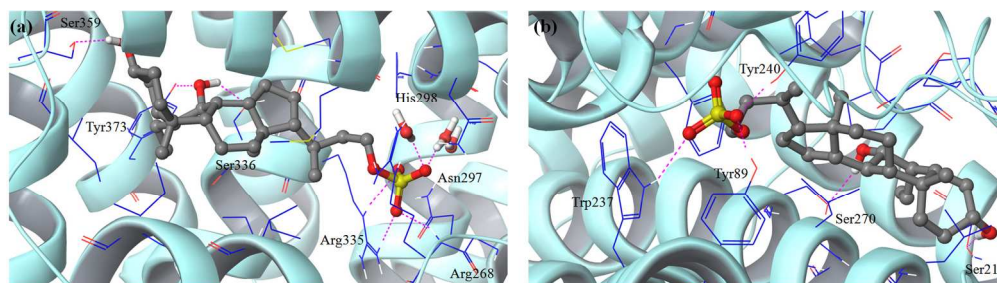
Figure 12: Total number of intermolecular hydrogen bonding interactions between four agonists in complex with TGR5

Figure 13: Min-6 cells treated with different concentration of ChemBridge_9149693 compound against uric acid induced oxidative damage and the cell viability was evaluated using MTT assay.

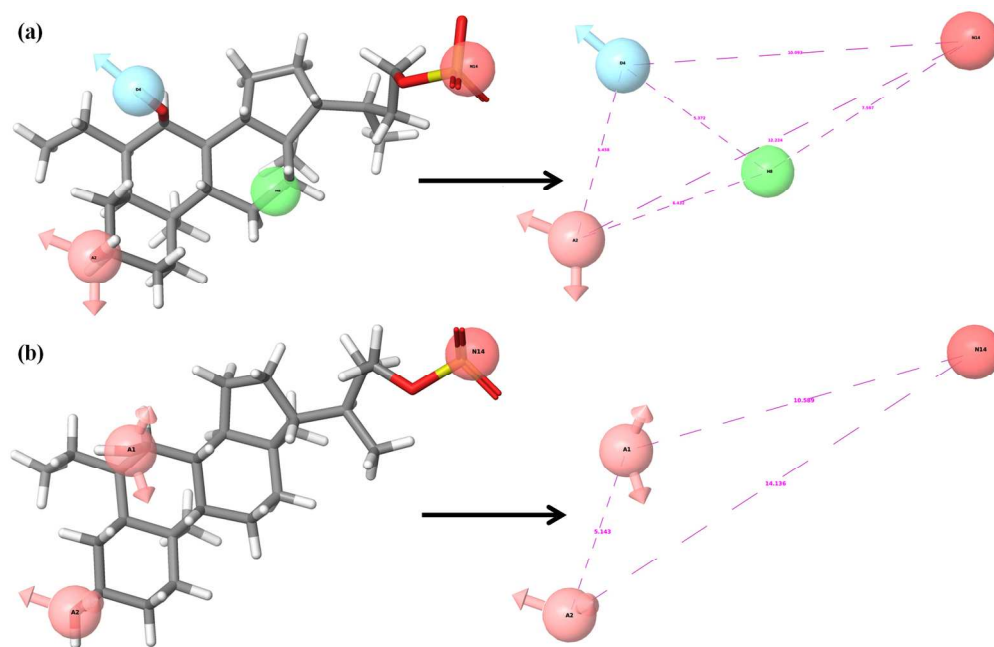
Figure 14: Fluorescence microphotograph of ROS generation in different groups including (a) control (b) uric acid-induced and (c) treatment with ChemBrigde_9149693.

Figure 15: The effect of two agonists on the activities of catalase (CAT) in uric acid-induced min-6 pancreatic β cells. Values are given as means \pm SD

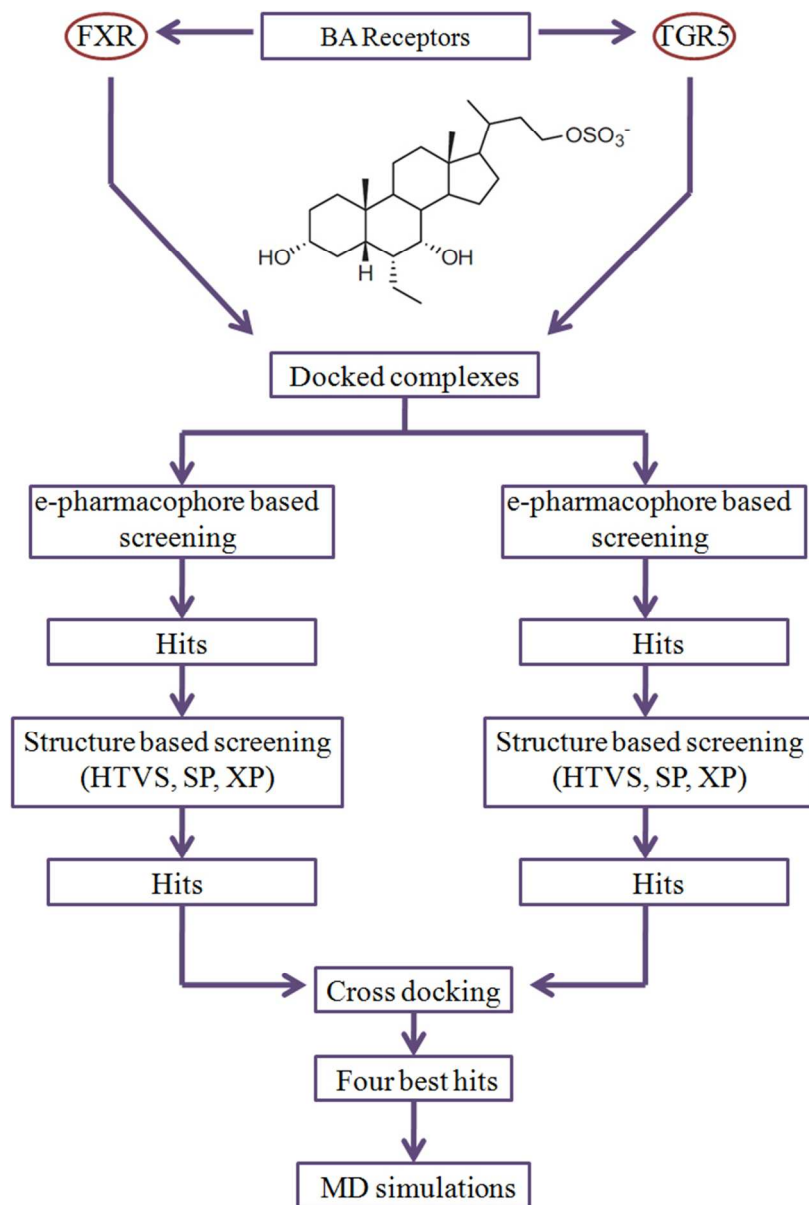
Figure 16: The effect of two agonists on the activities of Glutathione peroxide (GPx) in uric acid-induced min-6 pancreatic β cells. Values are given as means \pm SD



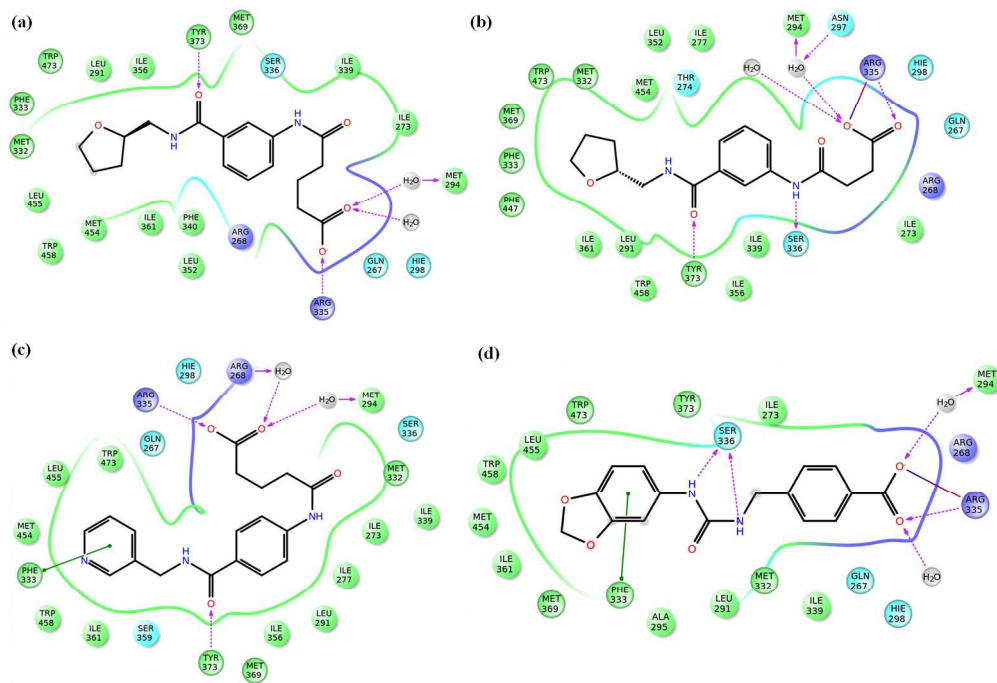
161x44mm (300 x 300 DPI)



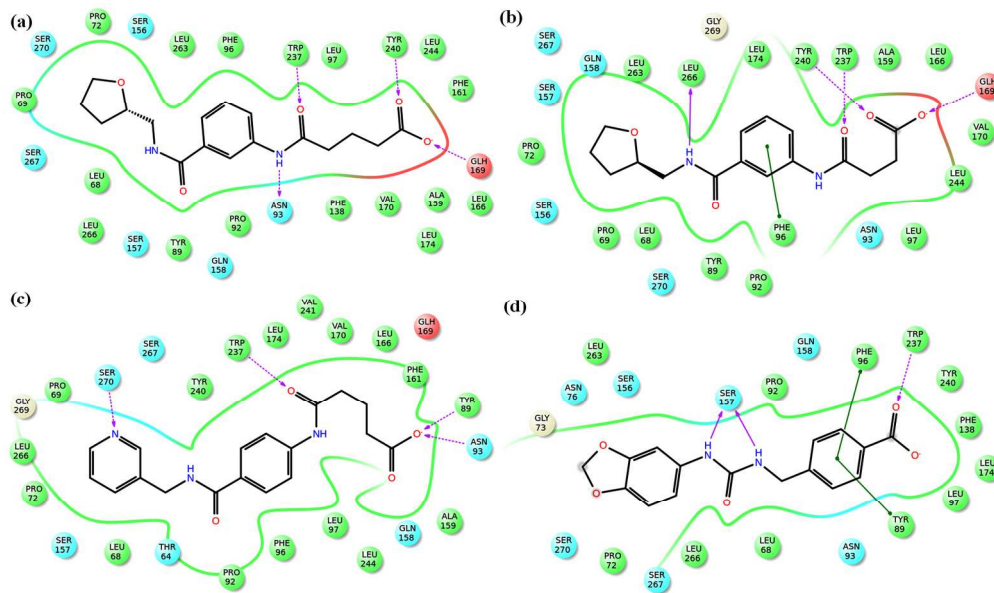
205x133mm (300 x 300 DPI)



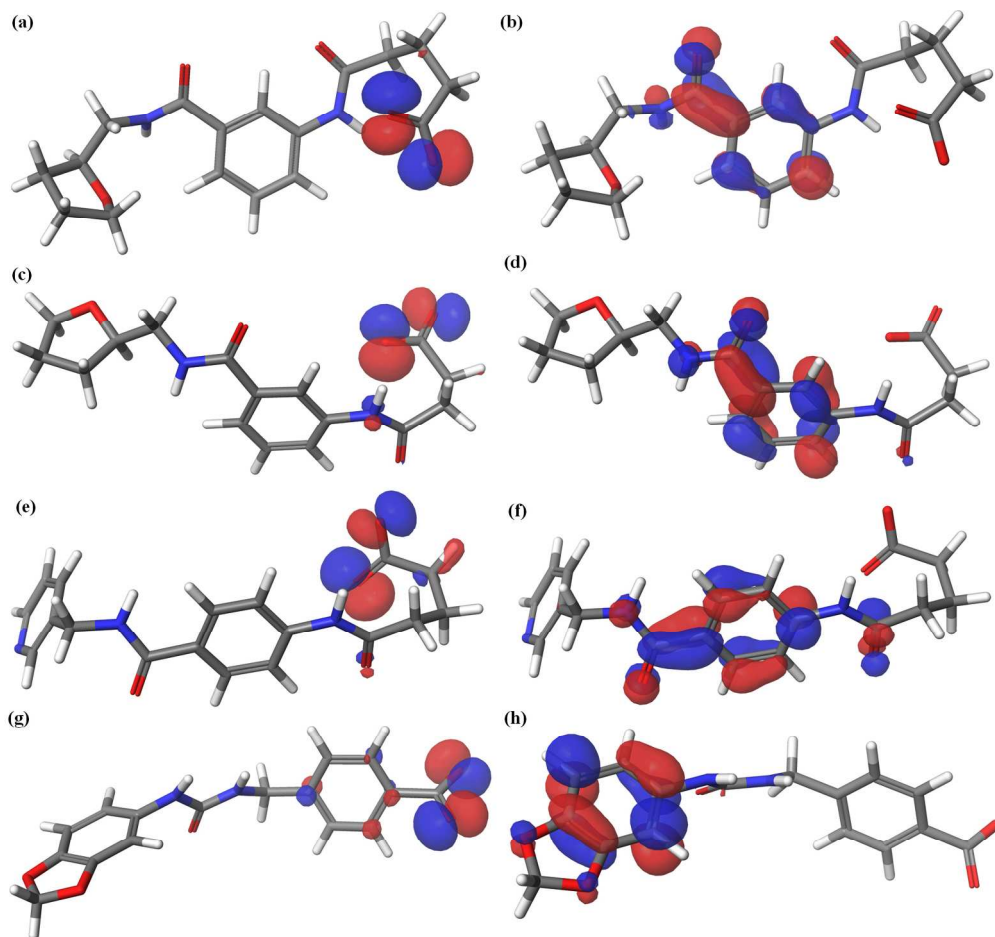
61x91mm (300 x 300 DPI)



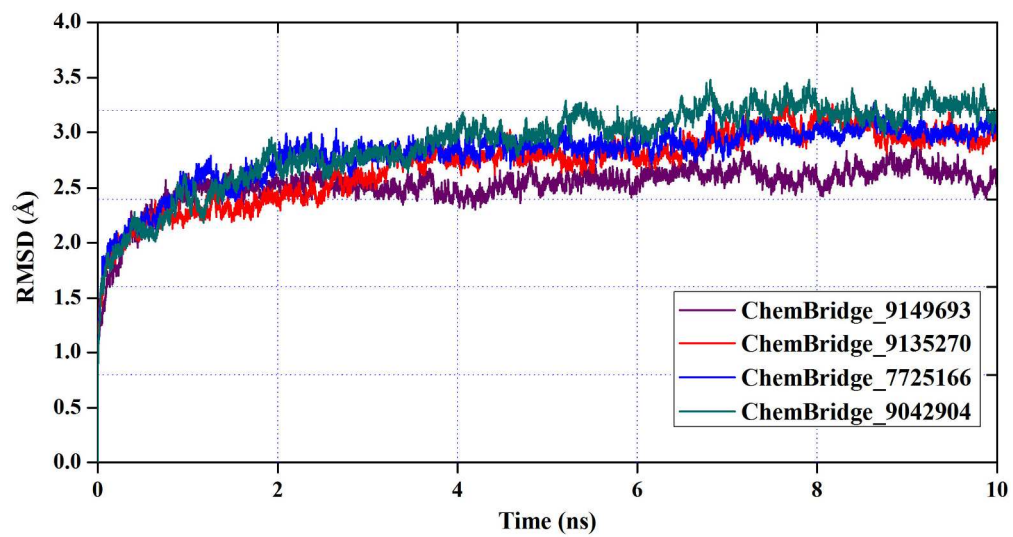
176x119mm (300 x 300 DPI)



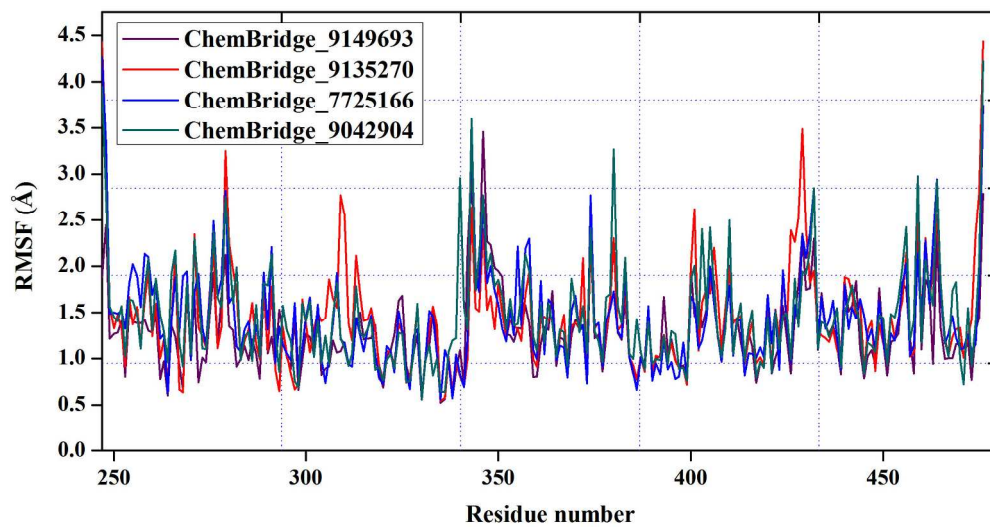
166x99mm (300 x 300 DPI)



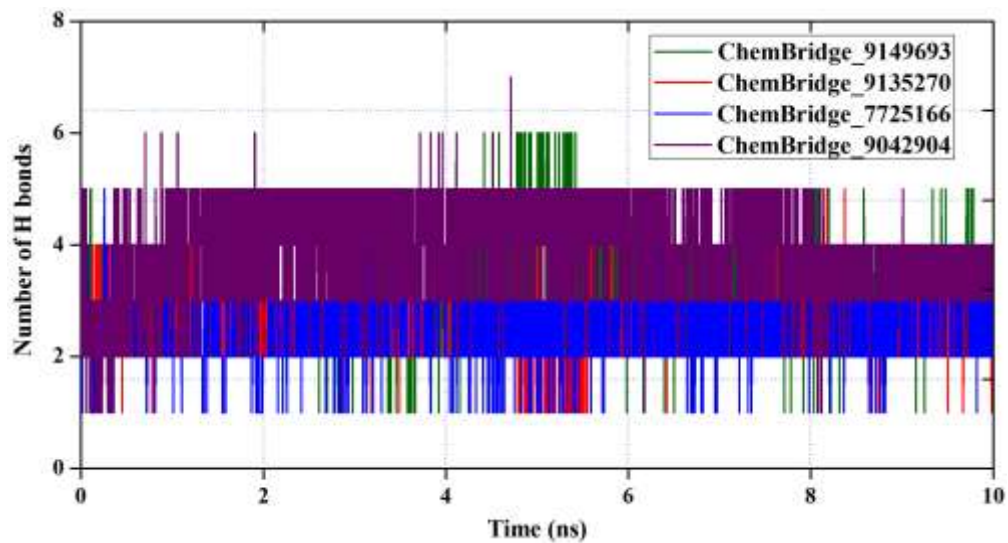
169x157mm (300 x 300 DPI)



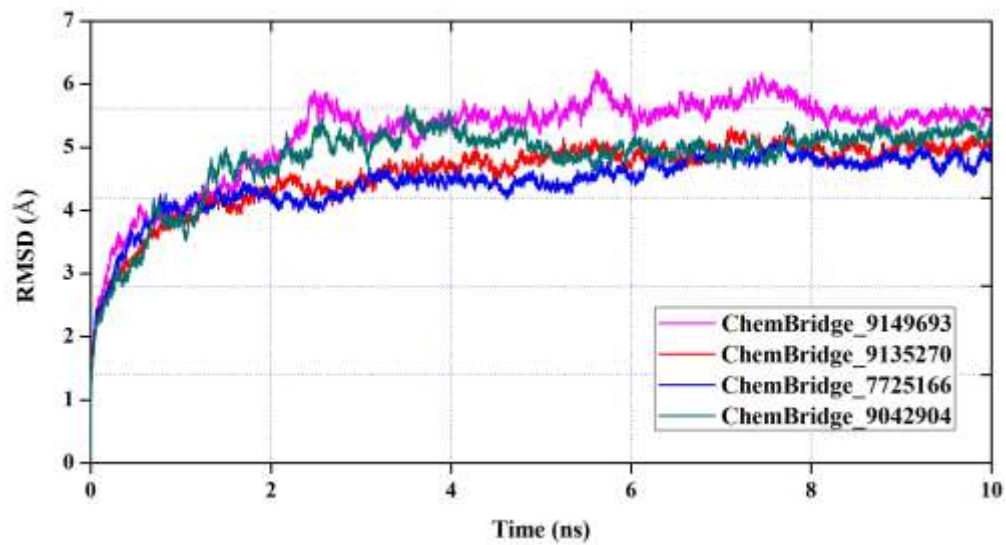
212x112mm (300 x 300 DPI)



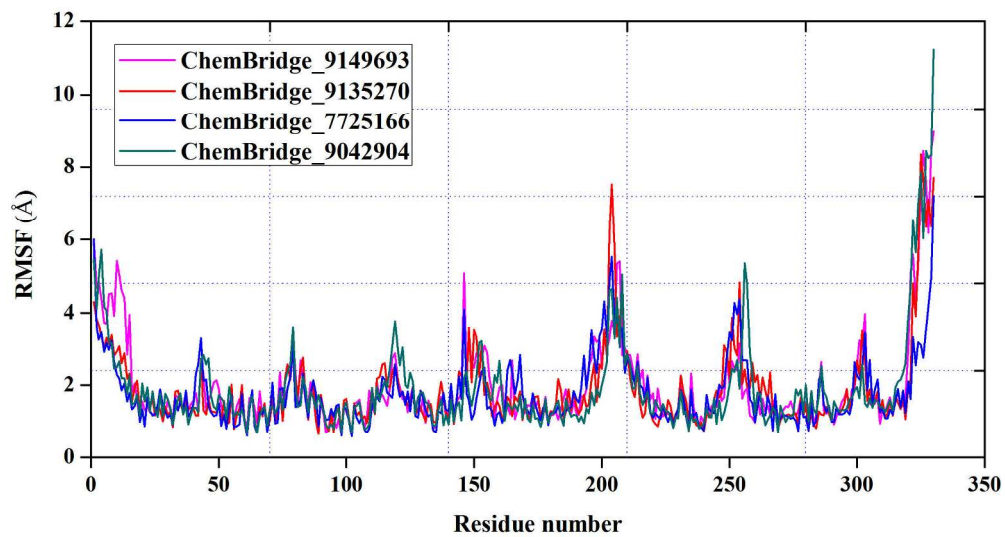
213x112mm (300 x 300 DPI)



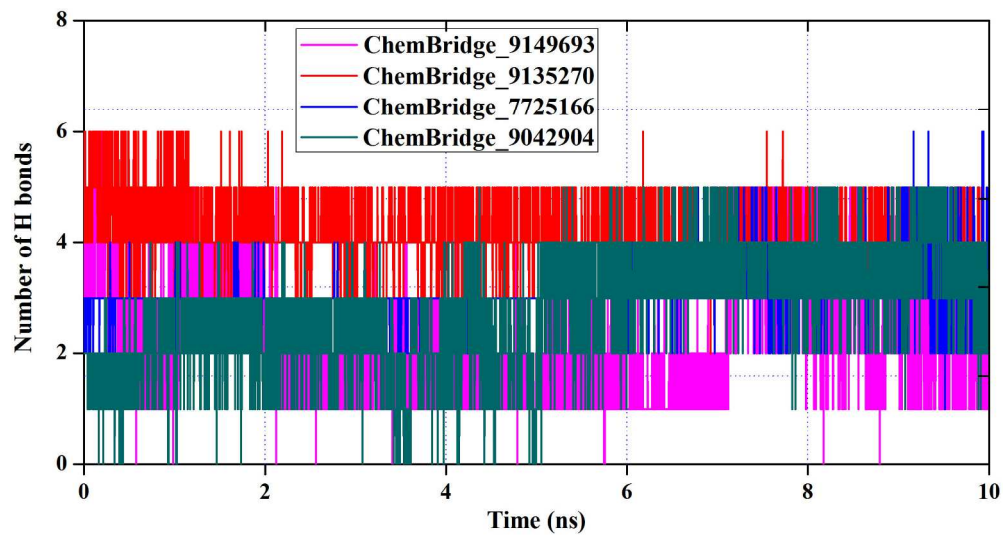
208x112mm (300 x 300 DPI)



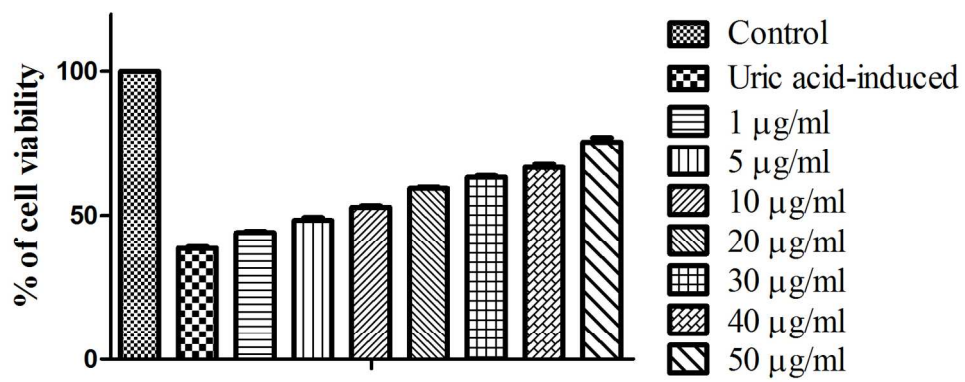
211x114mm (300 x 300 DPI)



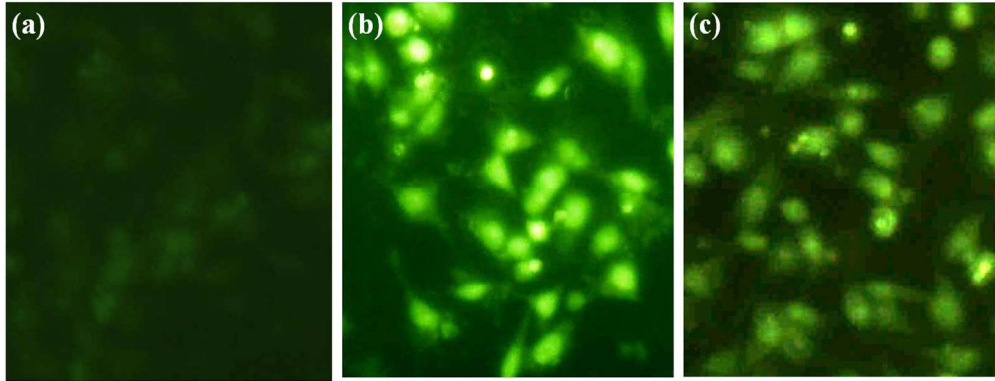
213x114mm (300 x 300 DPI)



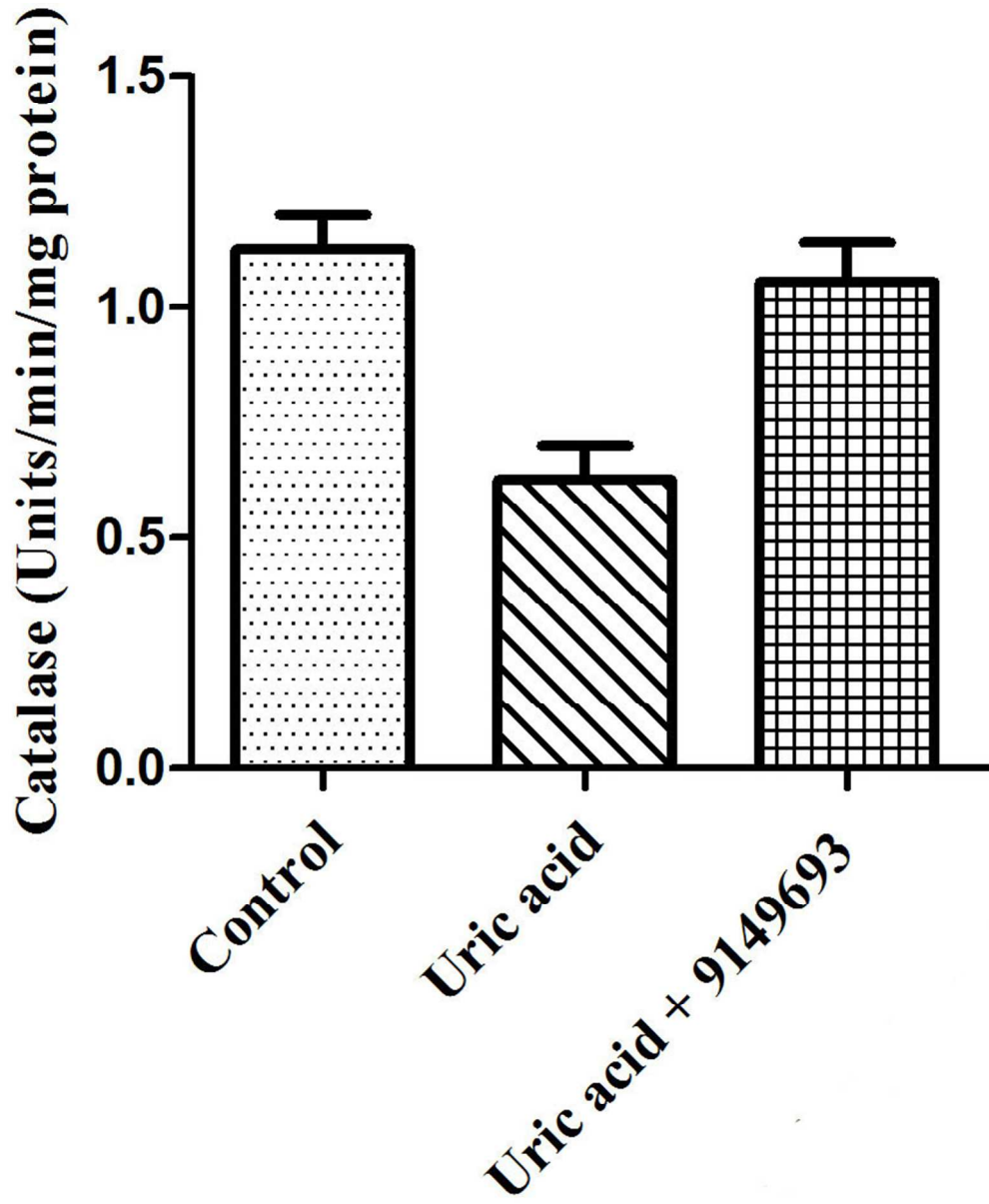
210x112mm (300 x 300 DPI)



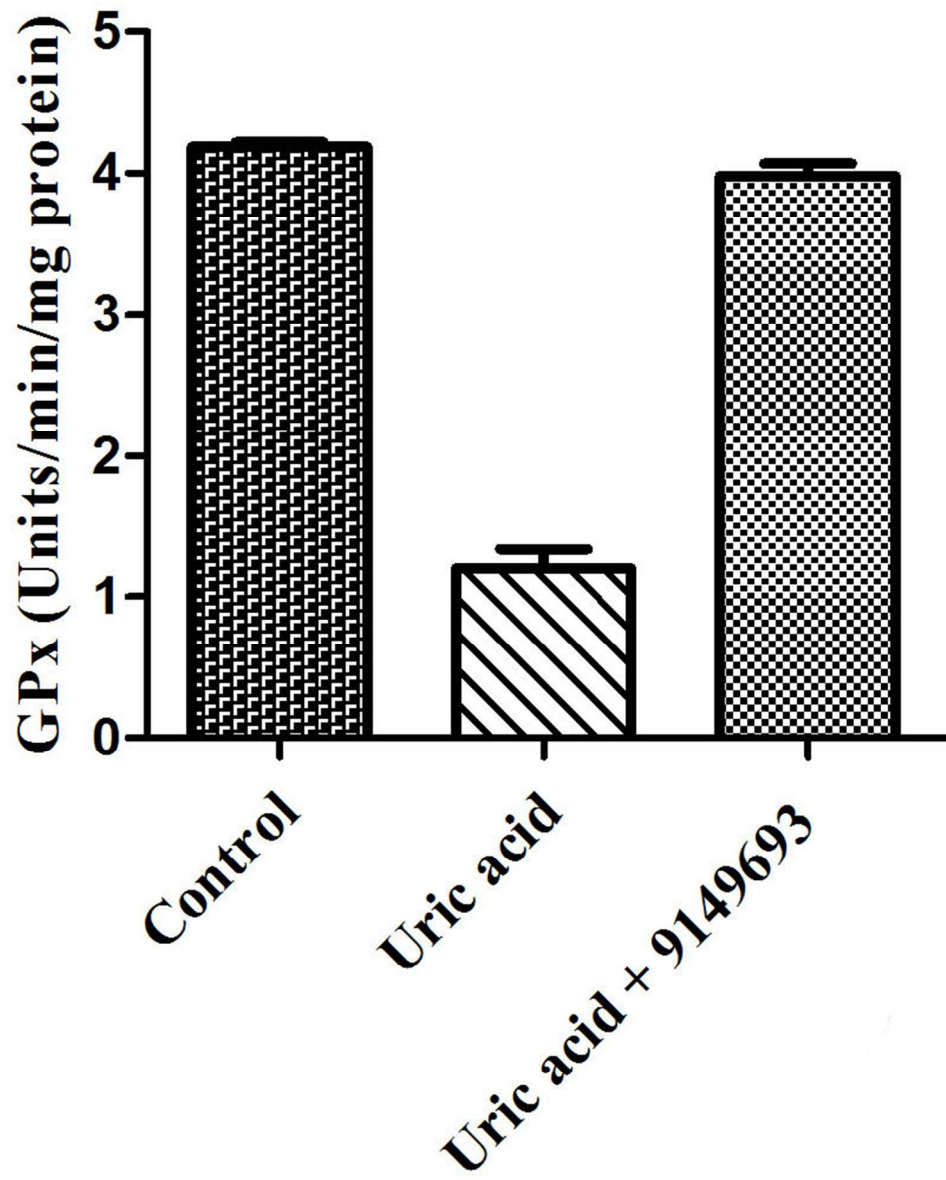
146x67mm (300 x 300 DPI)



139x53mm (300 x 300 DPI)



71x87mm (300 x 300 DPI)



71x84mm (300 x 300 DPI)